Numerical Calculation on Electromagnetic Energy Absorption in Pregnant Woman by RF Coil for MRI System

Satoru Kikuchi[1], Kazuyuki Saito[2], Masaharu Takahashi[2], Koichi Ito[1], and Hiroo Ikehira[3]

[1]*Graduate School of Engineering, Chiba University*
[2]*Research Center for Frontier Medical Engineering, Chiba University*
1-33 Yayoi-cho, Inage-ku, Chiba 263-8522, Japan
[1]kikuchi@graduate.chiba-u.jp
[3]*Natinal Institute of Radiological Sciences*
4-9-1 Anagawa, Inage-ku, Chiba 263-8555, Japan

***Abstract*— The numerical calculations including voxel human model with an anatomical structure for electromagnetic field and temperature rise induced by electromagnetic energy absorption have been widely investigated over the past dozen years or so. This paper presents the computational electromagnetic dosimetry inside an anatomically based pregnant woman models exposed to electromagnetic wave during magnetic resonance imaging. The two types of realistic woman models corresponding to early gestation and 26 weeks gestation were used for this study. The specific absorption rate (SAR) in and around a fetus were calculated by radiated electromagnetic wave from the birdcage coil with 1-port and 2-port feedings. Moreover, the temperature rise distributions in pregnant woman model due to the electromagnetic exposure are calculated by use of bioheat transfer equation. As the results of these calculations, the SAR and the temperature rise distributions inside the maternal body and her fetus are cleared.**

Key words: magnetic resonance imaging (MRI), birdcage coil, pregnant woman, fetus, finite difference time domain (FDTD) method, specific absorption rate (SAR), temperature rise

I. INTRODUCTION

In recent years, various types of devices based on electromagnetic techniques have been developed and used for various fields. Some of these devices are used in vicinity of a human body, therefore, there are become increasingly concerned about safety assessment associated with electromagnetic (EM) energy absorption. The health effects of the EM waves on the human body are dependent on frequency and strength of the waves [1]. In particular, above 100 kHz, the absorbed EM energy mainly contributes to the pyretic action. The specific absorption rate (SAR) has been standardly used as the primary dosimetric parameter for the EM wave exposure [2], [3]. Therefore, the SAR evaluation is an important research topic that needs to be taken into consideration by the World Health Organization (WHO) [4]. Meanwhile, it is well known that magnetic resonance imaging (MRI) is one of effective modalities, which can be obtained the anatomical image inside the human body by using the three types of EM field. Therefore, there have been increasing cases to use magnetic resonance (MR) imaging for pregnant woman and her fetus, because the MR imaging tends to generation of high quality images and reduction of acquisition time [5]. Therefore, it is necessary to evaluate the interaction between EM wave and a fetus.

Over the past few years, several studies have been made on the SAR evaluations of pregnant woman and her fetus due to the radiated EM energy from the RF coil [6]-[9]. These studies had a finite-difference time-domain (FDTD) method to calculate SAR in a voxel human model on pregnant woman. However, the basic restriction in the contemporary safety standards for MRI system has not specifically established for the pregnant woman and her fetus. On the other hand, several studies reported the results that thermal effect of the fetus causes growth delay and developmental defect [10]. According to ICNIRP (International Commission on Non-Ionizing Radiation Protection) report [11], it has been suggested that adverse effects on embryonic or fetal development will be avoided if the temperature of the fetus did not exceed 38 ^{o}C, and the body temperature of pregnant woman did not rise by more than 0.5 ^{o}C. There is a few In this study, the temperature rise distributions in the fetus due to the RF pulse radiation are calculated by use of the numerical calculation model assuming the actual MR imaging and the results are compared the recommended limits.

II. CALCULATION MODEL

A. Realistic Woman Model

In this calculation, two types of realistic woman models were employed. Figures 1 (a) and (b) show those models. Here, the whole-body voxel model with an adult Japanese female average figure is used for the calculation of the pregnant woman in early period (Model A). Moreover, the 26 gestational week pregnant woman model is applied as the last stage of pregnancy period (Model B). In addition, these models are composed of 2 mm ×2 mm × 2 mm cubical voxel and each voxel is assigned unique numbers corresponding to the tissue.

B. Calculation Model of Birdcage Coil

Figure 2 shows the birdcage coil used for the calculation. The operating frequency of the coil is around 64 MHz, which is used in the generic 1.5 T MRI systems to excite the nuclei in the human body for imaging. This coil consist of two end rings and eight legs, whose widths are 10 mm. Those elements are modeled as perfect electric conductor (PEC) for calculations. The diameter and the length of the coil are 600, 700 mm, respectively. In outside of the coil, the coils are surrounded by RF shield which is also modeled as PEC. A cylindrical RF shield, with an internal diameter of 740 mm and a length of 1,260 mm, has been located lateral to the coil. Here, the capacitors were loaded into the end rings on the birdcage coil in Fig. 2. In order to determine the capacitances, "birdcage builder [12]", which calculates the resonance frequency of the birdcage coil by the equivalent electrical circuit model, was employed.

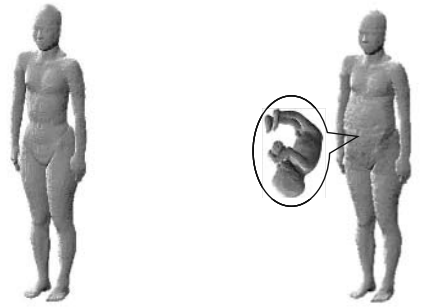

(a) Model A (b) Model B

Fig.1 Realistic woman models.

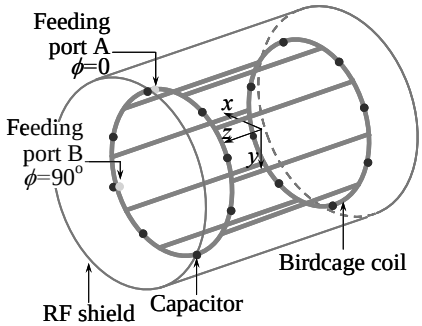

Fig. 2 Birdcage coil with RF shield.

C. Calculation Model including Birdcage Coil and Pregnant Woman Model

Figure 3 indicates an example of the FDTD calculation model including the realistic pregnant woman model (Model B). In order to calculate the whole-body of the woman models, a large analytical region was required. Therefore, we employed a super technical server (Hitachi SR11000) in the Institute of Media and Information Technology, Chiba University, for these calculations. In addition, the steady state analysis is performed by enforcing a continuous sinusoidal wave of electric field on the feeding gap to calculate the SAR distribution in the model. Moreover, the coordinate origin is the center of calculation model. In the numerical calculations, the non-uniform grids are employed and minimum size of grids same as resolution of woman model only for the coil and the model are used. The parameters used in the FDTD calculations are listed in Table I.

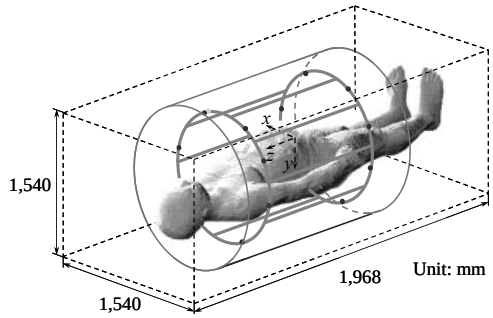

Fig. 3 FDTD calculation model.

TABLE I
PARAMETERS FOR FDTD CALCULATIONS

Minimum cell size [mm]	Δx, Δy Δz	2.0, 2.0 2.0
Maximum cell size [mm]	Δx, Δy Δz	5.6, 5.6 2.0
Analytical space $x \times y \times z$ [cell]		534 × 534 × 984
Time step [ps]		3.8
Absorbing boundary condition		PML (8 layers)

III. SAR AND TEMPERATURE CALCULATION TECHNIQUE

A. Calculation Technique for SAR

In this study, the SAR and temperature rise inside the body were calculated by use of the following equation. In order to calculate SAR inside the body due to the RF pulse radiation, electric field around the coil is analyzed by the FDTD method. This method is one of the EM analyses to calculate SAR inside a human body is well known as efficient technique. The SAR is calculated from the following equation:

$$\mathrm{SAR} = \frac{\sigma}{\rho} E^2 \quad [\mathrm{W/kg}] \qquad (1)$$

where σ is the conductivity of the tissue [S/m], ρ is the density of the tissue [kg/m^3], and E is the electric field (rms) inside the tissue [V/m].

B. Calculation Technique for Temperature Rise

The SAR is equivalent to the heating source generated by the electric field in the human tissue. In order to obtain the temperature distribution inside the body, we numerically analyze the bioheat transfer equation (BHE) [13] including the obtained SAR values using the finite difference method (FDM). The BHE is given by

$$\rho\, c \frac{\partial T}{\partial t} = \kappa \nabla^2 T - \rho \rho_b c_b F\left(T - T_b\right) + \rho \cdot \mathrm{SAR} \quad (2)$$

where T is the temperature [°C], t is the time [s], c is the specific heat of the tissue [J/kg·K], κ is the thermal conductivity of the tissue [W/m·K], ρ_b is the density of the blood [kg/m^3], c_b is the specific heat of the blood [J/kg·K], T_b is the temperature of the blood [°C], and F is the blood flow rate [m^3/kg·s]. The three terms on right-hand side of (2) represent heat diffusion through internal conduction, heat exchange due to capillary blood flow in each tissue, and heating source due to the

electromagnetic energy deposition, respectively. We substitute the SAR obtained by the previous electromagnetic analysis into the third term in the right-hand side of (2).

The BHE must be applied appropriate boundary condition to the surface of human body. Here, boundary condition for the body surface, which is defined by (3), is applied to simulate the thermal exchange.

$$\frac{\partial T}{\partial n} = \frac{h}{\kappa}\left(T_a - T_s\right) \qquad (3)$$

where n is the unit vector in the normal direction of the body surface, h is the convection coefficient [W/m^2·K], T_s is the surface temperature [^{o}C], and T_a is the fluid temperature [^{o}C]

In this study, we assumed that the temperatures of blood and fluid are equal to initial temperature of the tissue. The uniform grids were employed as this temperature calculation, because the calculation region should consider only around the body. In this case, the stability criterion of the temperature calculation was assumed to be (4) by referring to the paper by Wang *et al*. [14]

$$\Delta t \le \frac{2\rho c\delta^2}{12\kappa + \rho\rho_b c_b F\delta^2} \qquad (4)$$

where δ [m] is the cell size in the temperature calculation ($\delta = \Delta x = \Delta y = \Delta z$ [m]), and Δt [s] is the time step. The parameters used in the temperature calculations are listed in Table II. The values of convection coefficient and ambient temperature were taken from [8]. Here, the SAR and temperature calculations are performed by own developed code.

TABLE II
PARAMETERS FOR TEMPERATURE CALCULATIONS

Cell size : $\Delta x \times \Delta y \times \Delta z$ [mm]	2.0 × 2.0 × 2.0
Time step : Δt [s]	2.0
Convection coefficient h [W/m^2·K]	10.5
Ambient temperature [^{o}C]	24.0
Initial temperature [^{o}C]	37.0

IV. CALCULATED RESULTS

A. SAR Distributions

Figures 4 and 5 show the calculated SAR distribution by use of 1-port and 2-port feeding models, respectively. The observation planes are the coronal plane (xz-plane) including the uterus and around the center of the fetus in both cases. Here, the SAR values are normalized by 1.0 W radiated power from the coil. In addition, the radiation power was calculated by a surface integral of poynting vector on closed surface surrounding the coil. As shown in Figs. 4 and 5, relatively high SAR values are observed around the skin, muscle, etc which have a high electrical conductivity and are located close to the surface of the maternal body. Moreover, a high SAR value is observed inside of the thigh and axillars because of the existing narrow gap. Meanwhile, relatively high SAR values are observed around the border of amniotic fluid.

Moreover, compared with SAR distributions by different feeding point, it was confirmed that the SAR distributions in Fig. 5 are observed unsymmetrical. This is because the distribution is influenced by 2port feeding.

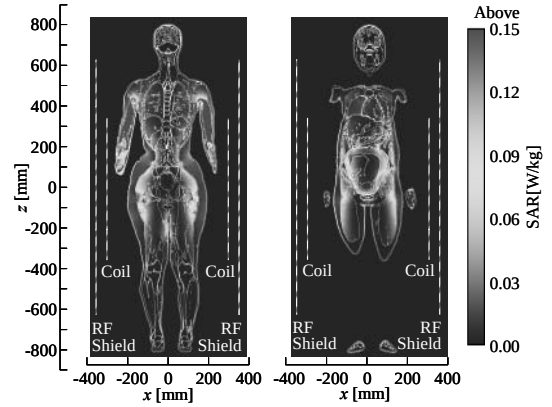

(a) Model A (b) Model B

Fig. 4 SAR distributions using 1-port feeding model.

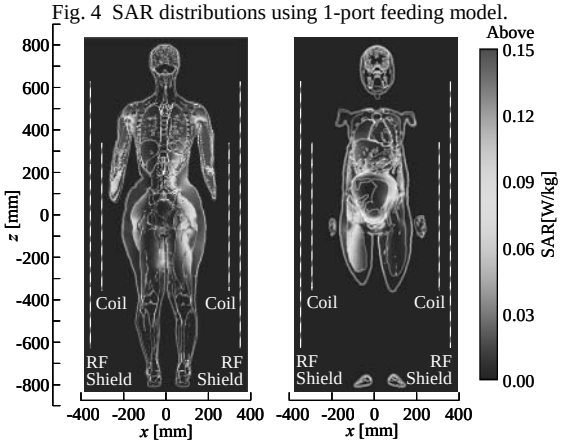

(a) Model A (b) Model B

Fig. 5 SAR distributions using 2-port feeding model.

B. Fetus and Uterus Average SAR

Figure 6 illustrates the calculated results of uterus or fetal average SAR inside Models A and B. Here, the weight of these models are 52.4 kg (in Model A) and 58.8 kg (in Model B), respectively. In this study, we curtailed about the discussion of whole-body average SAR, because whole-body average SAR was decided on two parameters; the one is the weight of human body, the others is radiation power from the coil. From Fig. 6, the values of uterus or fetal average SAR of 2-port feeding model are higher than that of 1-port feeding model.

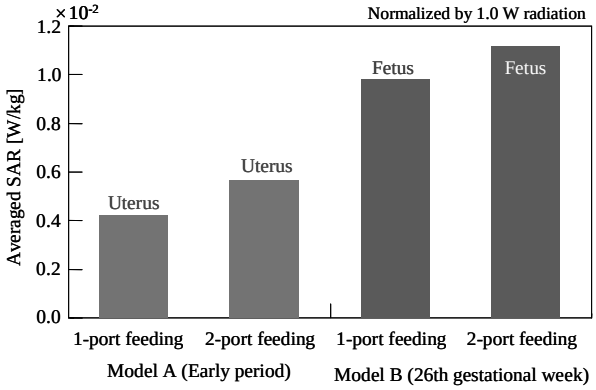

Fig. 6 Calculated average SAR by difference feeding point.

C. Temperature Distributions

Figures 7 and 8 show the calculated temperature rise distribution by different feeding port. Here, the positions of the observation plane are same as Figs. 4 and 5. In the temperature calculations, the SAR values are normalized to the whole-body average SAR limit in the IEC standard, which is 2 W/kg for normal operating mode. As shown in Figs. 7 and 8, it is confirmed that the temperature rise of the surface of the maternal body is low, because the temperature rise of the body surface is alleviated by difference of temperature with the ambient air. It is confirmed that temperature rise of the fat under the skin is high because of low specific heat.

Moreover, the temperature rise in and around the uterus and the fetus is low which compared the values of maternal body. According to ICNIRP report [11], the recommended limit of temperature in the fetus is 38.0 °C. In this study, maximum temperature in the fetus is about 37.5 °C. Therefore, it is confirmed that the maximum value in fetus is lower than that recommended value. In this study, although the SAR value of amniotic fluid surrounding fetus is relatively high, the temperature of the amniotic fluid was set to 37.0 °C to consider the effect of heat dissipation by convection. However, it must be investigated the validity, because the temperature in a fetus changes greatly related to applying this assumption.

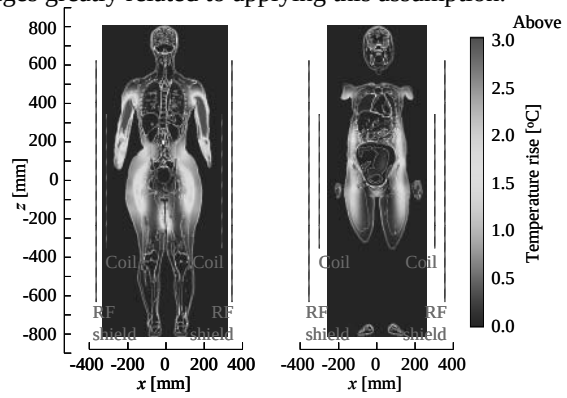

(a) Model A (b) Model B

Fig. 7 Temperature rise distributions using 1-port feeding model.

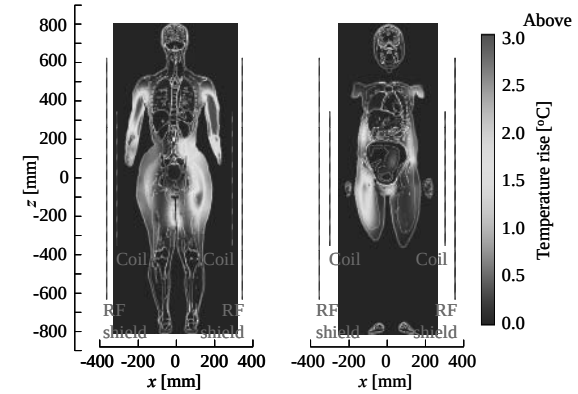

(a) Model A (b) Model B

Fig. 8 Temperature rise distributions using 2-port feeding model.

V. Conclusion

In this study, the SAR and the temperature rise distributions in two types of pregnant woman model were calculated during MR imaging. As a result of calculations, it has confirmed that the SAR value in the fetus is low in comparison with the SAR of maternal tissues. Moreover, it has also confirmed that the temperature in the fetus is lower than 38.0 °C which is recommended limit described in a literature. As further studies, it is necessary to calculate the SAR and temperature rise by the other RF coils used in conventional MRI systems. In addition, although the SAR and temperature distributions were calculated by a sinusoidal wave excitation in this study, the wave form of RF pluses must be considered for the actual imaging. Moreover, we will investigate a method to calculate the inside and outside of the amniotic fluid.

Acknowledgments

The authors would like to thank Dr. Tomoaki Nagaoka and Dr. Soichi Watanabe, National Institute of Information and Communications Technology, Tokyo Japan for their valuable comments in terms of using the realistic high-resolution whole-body voxel models.

References

[1] O. P. Gandhi, Strongest dependence of whole animal absorption on polarization and frequency of radio-frequency energy, *Ann. N. Y. Acad. Sci.*, vol. 247, pp. 532-538, Feb. 1975.

[2] ICNIRP, Guidelines for limiting exposure to time-varying electric, magnetic, and electromagnetic fields (0 Hz to 300 GHz), *Health Phys.*, vol. 74, no. 4, pp. 494-522, Apr. 1998.

[3] IEEE standard for safety levels with respect to human exposure to radio frequency electromagnetic fields, 3 kHz to 300 GHz, *ANSI/IEEE Standard* C95. 1-2005, Oct. 2005.

[4] "Research agenda of radio frequency fields," WHO, Geneva, Switzerland, 2006. [Online].Available: http://www.who.int/entity/peh-emf/research/rf_research_agenda_2006.pdf

[5] D. Levine, "Fetal magnetic resonance imaging," *Journal of Maternal-Fetal and Neonatal Medicine* vol. 15, no. 2, pp. 85-94, Feb. 2004.

[6] M. L. Strydom, K. Caputa, M. A. Stuchly, and P. Gowland "Numerical Modeling Interaction of RF Field in MRI with a Pregnant Female," IEEE/ACES Int. Wireless Communi. Appl. Computat. Electromagn. Conf., pp. 389-392, April 2005.

[7] J. W. Hand, Y. Li, E. L. Thomas, M. A. Rutherford, and J. V. Hajnal, "Prediction of specific absorption rate calculations in mother and fetus associated with MRI examinations during pregnancy," *Magn. Resonan. Med.*, vol. 55, pp. 883-893, 2006.

[8] D. Wu, S. Shamsi, J. Chen, and W. Kainz, "Evaluations of specific absorption rate and temperature increase within pregnant female models in magnetic resonance imaging birdcage coils," *IEEE Trans. Microw. Theory Tech.*, vol. 54, no. 12, pp. 4472-4478, Dec. 2006.

[9] S. Kikuchi, K. Saito, M. Takahashi, K. Ito, and H. Ikehira, "SAR computation inside fetus by RF coil during MR imaging employing realistic numerical pregnant woman model," *IEICE Trans. Commun.* vol. E92-B, no.2, Feb. 2009. (in press)

[10] J. M. Graham, M. J. Edwards, and M. J. Edwards "Teratogen update: Gestational effects of maternal hyperthermia due to febrile illnesses and resultant patterns of defects in humans," *Teratology*, vol. 58, pp. 209-221, 1998.

[11] ICNIRP, Medical Magnetic Resonance (MR) procedures: protection of patients, Health Physics, vol. 87, no. 2, pp. 197-216, Aug. 2004.

[12] C. L. Chin, C. M. Collins, S. Li, B. J. Dardzinski, M. B. Smith, Bird cage Builder, version 1.0 Copyright Center for NMR Research, Department of Radiology, Penn State University College of Medicine, 1998.

[13] H. H. Pennes, "Analysis of tissue and arterial blood temperatures in the resting human forearm," Journal of Applied Physiology, vol. 1, pp. 93–122, Aug. 1948.

[14] J. Wang and O. Fujiwara, "FDTD computation of temperature rise in the human head for portable telephones," *IEEE Trans. Microw. Theory Tech.*, vol. 47, pp. 1528–1534, Aug. 1999.